



2014

# Microwave plasmas applied for the synthesis of free standing graphene sheets

Tatarova, E.

---

J. Phys. D: Appl. Phys. 47 (2014) 385501 (11pp)  
<http://hdl.handle.net/10945/43441>



Calhoun is a project of the Dudley Knox Library at NPS, furthering the precepts and goals of open government and government transparency. All information contained herein has been approved for release by the NPS Public Affairs Officer.

**Dudley Knox Library / Naval Postgraduate School**  
**411 Dyer Road / 1 University Circle**  
**Monterey, California USA 93943**

# Microwave plasmas applied for the synthesis of free standing graphene sheets

E Tatarova<sup>1</sup>, A Dias<sup>1</sup>, J Henriques<sup>1</sup>, A M Botelho do Rego<sup>2</sup>, A M Ferraria<sup>2</sup>, M V Abrashev<sup>3</sup>, C C Luhrs<sup>4</sup>, J Phillips<sup>5</sup>, F M Dias<sup>1</sup> and C M Ferreira<sup>1</sup>

<sup>1</sup> Institute of Plasmas and Nuclear Fusion, Instituto Superior Técnico, University of Lisbon, Portugal

<sup>2</sup> Centro de Química-Física Molecular and IN, Instituto Superior Técnico, University of Lisbon, Portugal

<sup>3</sup> Faculty of Physics, Sofia University, 1164 Sofia, Bulgaria

<sup>4</sup> Department of Mechanical and Aerospace Engineering, Naval Postgraduate School, Monterey, CA 93943, USA

<sup>5</sup> Department of Physics, Naval Postgraduate School, Monterey, CA 93943, USA

E-mail: [e.tatarova@ist.utl.pt](mailto:e.tatarova@ist.utl.pt)

Received 15 March 2014, revised 11 July 2014

Accepted for publication 25 July 2014

Published 22 August 2014

## Abstract

Self-standing graphene sheets were synthesized using microwave plasmas driven by surface waves at 2.45 GHz stimulating frequency and atmospheric pressure. The method is based on injecting ethanol molecules through a microwave argon plasma environment, where decomposition of ethanol molecules takes place. The evolution of the ethanol decomposition was studied *in situ* by plasma emission spectroscopy. Free gas-phase carbon atoms created in the plasma diffuse into colder zones, both in radial and axial directions, and aggregate into solid carbon nuclei. The main part of the solid carbon is gradually withdrawn from the hot region of the plasma in the outlet plasma stream where nanostructures assemble and grow. Externally forced heating in the assembly zone of the plasma reactor has been applied to engineer the structural qualities of the assembled nanostructures. The synthesized graphene sheets have been analysed by Raman spectroscopy, scanning electron microscopy, high-resolution transmission electron microscopy and x-ray photoelectron spectroscopy. The presence of sp<sup>3</sup> carbons is reduced by increasing the gas temperature in the assembly zone of the plasma reactor. As a general trend, the number of mono-layers decreases when the wall temperature increases from 60 to 100 °C. The synthesized graphene sheets are stable and highly ordered.

Keywords: graphene, microwave plasma, ethanol

(Some figures may appear in colour only in the online journal)

## 1. Introduction

Graphene possesses many extraordinary properties [1, 2], with potential applications in numerous scientific and engineering disciplines, including electronic devices, transparent conductive films, mechanical devices, chemical sensors, energy conversion and storage applications, etc [1–6]. Electrical, mechanical and optical performances of graphene crucially depend on its structural characteristics, i.e., number of mono-layers, presence of sp<sup>3</sup> carbons, defects etc. Normally, the structural properties of nanostructures and, in particular, of graphene, essentially depend on the assembly pathway. The reported methods for graphene synthesis correspond to either

‘top-down’ or ‘bottom-up’ approaches. Graphene of the highest quality can be obtained by mechanically exfoliating highly oriented pyrolytic graphite which can be considered the most used example of the first approach. Unfortunately this method cannot yet be scaled up for commercial applications. The generation of graphene oxide from graphite and the thermal reduction of the former is a second example of a top-down strategy; however despite rendering much higher yields, the method produces a highly defective product [7]. Bottom-up approaches include epitaxial growth, chemical vapour deposition (CVD) and vacuum graphitization of silicon carbide substrates, among others [2, 8–10]. The synthesis of graphene by CVD requires multiple processing steps, such

as wet-etching and micro-fabrication, to obtain transferable sheets [8–11]. This has driven a search for an alternative technique capable of providing high yields of clean and highly ordered graphene sheets with well controlled structural qualities. Plasma-based methods demonstrate a high potential towards these goals.

As compared with conventional neutral gas-based processes, plasma-based processes offer several advantages [12, 13]. The principal one is the very high and highly controllable energy density in the processing area, which allows effective control over the energy and material supply to the nanostructures via proper selection of the plasma parameters. Plasma systems provide simultaneously high temperatures and a highly reactive environment with many active species, e.g., electrons, ions, free radicals, highly energetic photons, which may strongly influence the assembly pathways across different temporal and space scales, including the atomic ones. In this way, the remarkable potential of plasmas allows to implement singular assembly pathways and unique atomic-level arrangements of nanostructures [4, 12–14]. Many of the current plasma techniques aimed at synthesizing carbon nanostructures involve plasma enhanced CVD (PECVD) [11, 13]. PECVD methods, as a rule, require low-pressure environments (below 10 Torr) and the use of substrates to obtain carbon nanostructures. The synthesis and growth of these structures proceed via surface reactions and depend, therefore, on substrate conditions.

Recent developments suggest that microwave plasma processing through the so-called aerosol-through-plasma (A-T-P) method [15–20] can be used to produce structures of interest in many fields, including catalysis, high energy density batteries and other forms of energy storage. In this technique, precursors, which can be particles, liquids, or even gases, are carried through a high temperature microwave plasma zone generally at, or near, atmospheric pressure. This method has also been applied to synthesize substrate-free graphene sheets [4, 18–20]. As shown in our previous work [21], tuning of the plasma properties and, in particular, of its afterglow conditions is of considerable importance to establish a control on the processes of nucleation and growth of the nanostructures and on the morphology of the targeted structures.

The present investigation exceeds our previous work [19, 21] on the creation of self-standing graphene sheets using microwave atmospheric plasmas driven by surface waves at atmospheric pressure conditions. The method is based on injecting a carbon containing precursor, such as ethanol molecules through a microwave argon plasma environment, where decomposition of such molecules takes place and atomic carbon is created. Gas-phase carbon atoms diffuse into colder zones both in radial and axial directions and as a result gas-phase carbon is transformed into solid carbon nuclei. A part of the solid carbon is deposited on the discharge tube wall while the main part is gradually withdrawn from the hot region of the plasma in the outlet gas stream, where nanostructures are assembled. It has been demonstrated in [21] that externally forced cooling/heating in the assembly zone of the plasma reactor results in different carbon nanostructures synthesis such as carbon nanoparticles at wall temperatures as low as

0 °C and graphene sheets at temperatures greater than 60 °C. Here, we extend our previous investigations to engineer the structural properties of produced graphene sheets via mastering the thermodynamic conditions in the assembly zone of the plasma reactor. For this reason additional forced heating in the assembly zone has been applied. In addition to Raman spectroscopy, scanning electron microscopy (SEM), high-resolution transmission electron microscopy (HRTEM) and x-ray photoelectron spectroscopy (XPS) elemental analysis has also been performed. Correlation between the Raman spectroscopy and XPS spectroscopy results was found. External forced heating in the assembly zone results in a decrease of the amount of  $sp^3$  carbons and an increase of the  $sp^2$  bonded hexagonal structures typical of graphene sheets. The experimental proof of this concept can be found by analysing the ratio of D-peak to the G-peak intensities detected in the Raman spectra, commonly associated with the degree of disorder [22]. Moreover, the detected delocalization of  $\pi$  electrons shifts from about 4.5 to about 6 eV supporting the above findings.

## 2. Experimental

### 2.1. Experimental setup and conditions

A surfatron-based setup was used to create surface wave induced microwave plasma at atmospheric pressure conditions [23]. The microwave power is provided by a 2.45 GHz generator (Sairem), whose output power was varied from 500 to 900 W. The discharge takes place inside a quartz tube with internal and external radii of 7.5 and 9 mm, respectively, which is inserted vertically and perpendicularly to the waveguide wider wall. The background argon gas is injected into the discharge tube at flow rate  $\Phi_{Ar} = 250$  sccm under laminar gas flow conditions. The precursor partial flux ( $\Phi_{Et}$ ) was varied in the range 0.6–3.5 sccm. Vaporization is performed by passing argon gas through a tank with liquid ethanol of 99.99% purity, with accurate control of the temperature. The partial ethanol flow has been changed via rigid temperature control of the liquid in the tank. This procedure was experimentally calibrated, whose validity was checked against Clausius–Clapeyron law. The total flow passing through the discharge consists of the direct argon flow plus the combined flows of the argon bubbling in the precursor liquid and the vaporized precursor. The wall temperature in the assembly zone of the plasma reactor, i.e., the plasma afterglow zone, was actively controlled by a cryostat system. The cooling/heating fluid circulates, with a constant flow rate, between the cryostat and a tubular heat exchanger as shown in figure 1. The heat exchanger (of 20 cm in length) is placed immediately after the end of the discharge zone, whose length is about 10–12 cm as seen in figure 1. The nanostructures were captured by a membrane filter system coupled to an Edwards BS2212 two-stage vacuum pump.

For gas sampling, a portion of the output gas stream from the plasma reactor (close to the remote plasma afterglow region) was directed to a Fourier transform infrared (FT-IR) Termo Nicolet 5700 spectrometer and the absorption

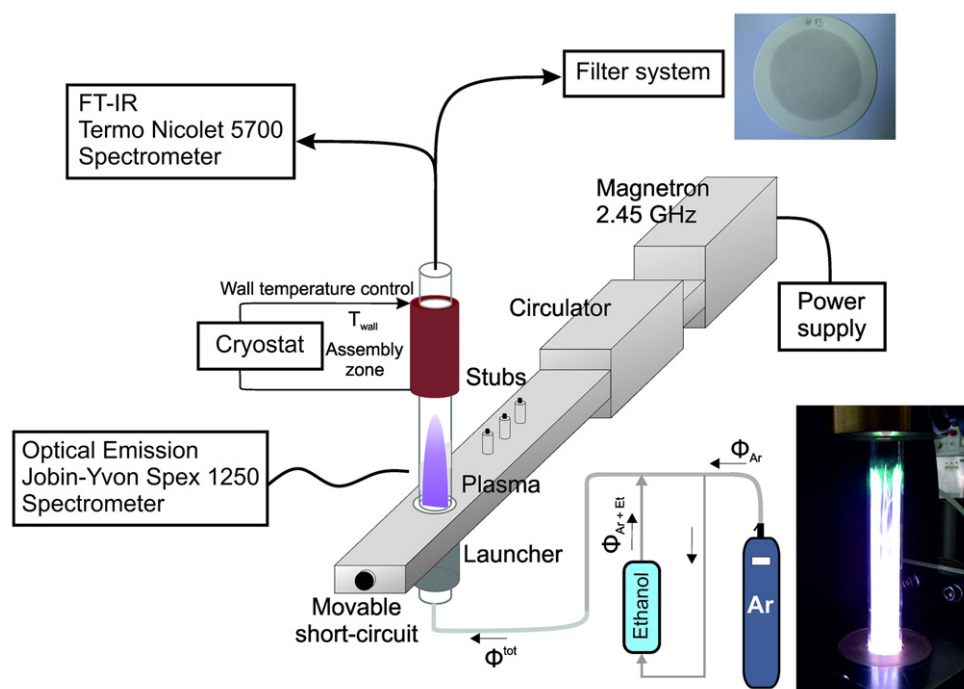


Figure 1. Experimental setup.

spectra of species was detected in the wave number range  $1000\text{--}4000\text{ cm}^{-1}$ . The light emitted by the plasma was collected perpendicularly to the discharge tube by an imaging optical fibre and directed to the entrance of a Jobin-Yvon Spex 1250 spectrometer ( $2400\text{ g mm}^{-1}$  grating) equipped with a charge-coupled device (CCD) camera. The cryogenic, back illuminated UV sensitive CCD camera has a  $2048 \times 512$  matrix, featuring a  $13.5\text{ }\mu\text{m}$  pixel-size, which provides high spectral resolution. The plasma emission spectra in the  $230\text{--}750\text{ nm}$  range have been detected.

## 2.2. Samples characterization

**2.2.1. HRTEM and scanning electron microscopy** The synthesized graphene flakes were placed either directly as a solid powder or in a diluted methanol dispersion onto a holey grid of a 200 kV JEOL 2010 transmission electron microscope (TEM). The graphene nanosheets have been further characterized by high-resolution TEM. HRTEM was performed with a Titan ChemiStem (FEI) HRTEM operating at 200 kV accelerating voltage.

SEM characterization of the samples was performed by a JEOL, JSM-7001F field emission gun scanning electron microscope operating in secondary electron imaging mode (SEI) with applied voltages in the range of  $10\text{--}15\text{ kV}$ .

**2.2.2. Raman spectroscopy analysis.** In order to perform Raman spectroscopy characterization, the synthesized nanostructures were freely suspended on a glass substrate and the Raman spectra from different regions on the substrate were obtained using a LabRAM HR Visible (Horiba Jobin-Yvon) Raman spectrometer at  $633\text{ nm}$ , with a  $5\text{ cm}^{-1}$  spectral resolution and laser spot size of  $2\text{ }\mu\text{m}$ . Measurements were

performed with a laser power  $P_l = 0.054\text{ mW}$  to avoid overheating.

**2.2.3. X-ray photoelectron spectroscopy.** XPS spectra were obtained with a KRATOS XSAM800 x-ray spectrometer with a double anode, operating in fixed analyser transmission mode, with an analyser pass energy of  $20\text{ eV}$  and non-monochromatic x-radiation with a power of  $120\text{ W}$  ( $12\text{ kV} \times 10\text{ mA}$ ). Samples were analysed at room temperature, at UHV pressure around  $10^{-7}\text{ Pa}$  and a take-off angle set to  $90^\circ$ . Graphene sheets were peeled from the filters using the XPS sample holder with double-sided tape. The spectra were collected in  $0.1\text{ eV}$  steps, using a Sun SPARC Station 4 with Vision software (Kratos). X-ray source satellites were subtracted. Shirley backgrounds and Gaussian/Lorentzian line shapes were fitted using XPS Peak 4.1 (freeware). No flood gun was used for charge compensation. Binding energies (BEs) were corrected taking as a reference the BE of  $\text{sp}^2$  carbons. For quantitative purposes, sensitivity factors were 0.25 for C 1s and 0.66 for O 1s.

## 3. Results and discussion

### 3.1. Plasma source characterization

The 'active' microwave plasma region of the reactor considered (figure 1) is composed of two zones. The first one is the surface wave sustained discharge zone, including the zone inside the launcher and the extended 'hot' plasma zone outside the launcher. Here, the surface wave power is absorbed by plasma electrons, which transfer the power to heavy particles via elastic and inelastic collisions, with high gas temperatures (up to  $3000^\circ\text{K}$ ) being achieved. The gas temperature keeps

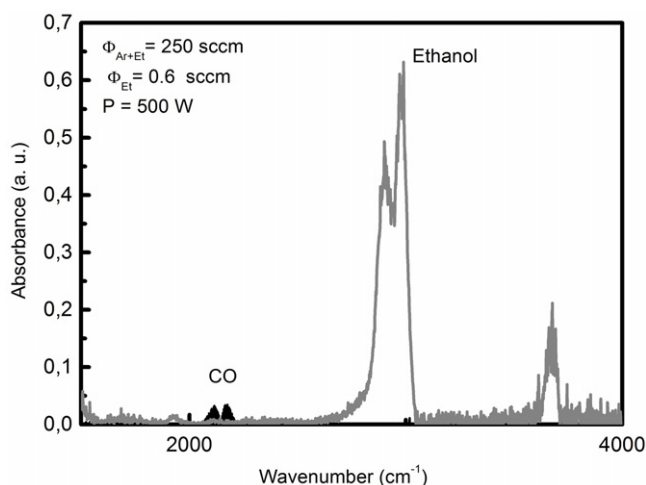


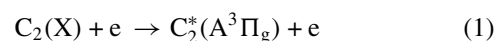
**Figure 2.** Infrared spectra of the outlet gas stream. Plasma off—grey line; plasma on—black line.

nearly constant in the discharge zone when moving away from the launcher (up to about 10 cm) and then drops sharply in the ‘near’ (~13 cm) afterglow plasma zone [24, 25]. It should be noted that the gas temperature is also radially inhomogeneous, with a radial profile close to the parabolic one. These two regions (~13 cm) form the ‘active/hot’ plasma zone, where the ethanol molecules are decomposed into simple atoms and molecules (C, H, H<sub>2</sub>, C<sub>2</sub>, CO). Over a time scale on the order of 10<sup>-2</sup> s, ethanol molecules dissociate in the hot plasma zone and solid carbon nuclei are formed. The next final zone is the ‘assembly zone’ (see figure 1) where kinetic processes of assembly and growth take place. Infrared sensitive measurement of the wall temperature axial profile using an optical thermometer has been performed in two cases, namely with and without a connected heat exchanger, i.e., with and without forced heating being applied to the assembly zone of the reactor. It should be stressed that the presence of the heat exchanger that fixes the wall temperature profile in the assembly zone does not influence the wall temperature profile in the hot plasma zone.

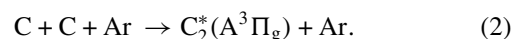
Mass and (FT-IR) spectroscopy have been applied to analyse the plasma outlet gas stream. Hydrogen and carbon monoxide are the main gas products of ethanol decomposition in the argon plasma environment [26]. To monitor the ethanol molecules decomposition processes FT-IR analysis of the argon/ethanol outlet gas stream has been performed when the plasma is turned on or off (figure 2). The absorption spectra detected without plasma showed spectral lines at around 2900 and 3700 cm<sup>-1</sup>, which are ‘finger prints’ of ethanol molecules. With the plasma turned on these lines are not present, clearly indicating that the ethanol molecules are decomposed in the argon plasma environment. Simultaneously, the absorption peak of CO at about 2170 cm<sup>-1</sup> is detected.

Plasma emission spectroscopy has been applied to identify species of interest and to determine the gas temperature in the discharge ‘hot’ zone. In fact, optical emission spectroscopy permits to identify the active species present in the plasma during the synthesis and growth of the carbon nanostructures in the outlet plasma stream. The detected plasma emission

spectra in the visible range are shown in figure 3. The emission of C<sub>2</sub>(A<sup>3</sup>Π<sub>g</sub> → X<sup>1</sup>Π<sub>u</sub>) (Swan system, between 4500–5700 Å) and OH (A<sup>2</sup>Σ<sup>+</sup>, v = 0 → X<sup>2</sup>Π<sub>i</sub>, v' = 0) (3000–3200 Å) bands has been detected. The emission band from NH(A<sup>3</sup>Π → X<sup>3</sup>Σ<sup>-</sup>) transitions at 3360 Å, from CN species corresponding to violet CN(B<sup>2</sup>Σ<sup>+</sup> → X<sup>2</sup>Σ<sup>+</sup>) transitions as well as the Fulcher-α band have also been detected. The experiments were carried out in the open atmosphere so that nitrogen containing species also appear. The detected emission of carbon atoms at 2479 Å, the main species of interest for the synthesis of carbon nanostructures, is to be noticed. As it can be seen in figure 3, strong plasma emissions of C<sub>2</sub> molecular bands, i.e., the Swan system, with head bands at 4737, 5165 Å and 5586 Å were detected. The typical C<sub>2</sub> emission is generated by the radiative decay of the C<sub>2</sub><sup>\*</sup>(A<sup>3</sup>Π<sub>g</sub>) state. Due to the low energy threshold (E<sub>ext</sub> = 2.4 eV), ground state C<sub>2</sub> molecules can easily be excited to this level either by electron impact [27]



or by three body recombination processes involving C and Ar atoms



Reactions of C<sub>2</sub> molecules with H, O radicals result in C<sub>2</sub> dissociation and formation of atomic carbon.

In discharges at atmospheric pressure, the rotational temperature can usually be assumed to be equal to the gas temperature [24, 25]. In this work, the intensity of the Q<sub>1</sub> branch of the OH band was used to estimate the rotational temperature. An estimation of the gas temperature was obtained from measurements of the rotational OH (A<sup>2</sup>Σ<sup>+</sup>, v = 0 → X<sup>2</sup>Π<sub>i</sub>, v' = 0) (3000–3200 Å) spectra assuming local thermodynamic equilibrium between rotational and translational degrees of freedom. The rotational temperature measured in this way at z = 2 cm distance from the launcher (nearly at the middle of the ‘hot’ plasma zone) was found to increase linearly from 1300 K to nearly 2000 K when the microwave power increases from 300 to 900 W (Φ<sub>Ar</sub> = 250 sccm; Φ<sub>Et</sub> = 0.6 sccm). It should be mentioned that this temperature corresponds to the axial part of the ‘hot’ plasma column as far as the radiation collected originates mainly from this region. The axial variations of the OH rotational temperature were presented in [24, 28].

### 3.2. Parametric study

The ability to control the local area where energy and matter are delivered from the bulk plasma to the developing nanostructures is the key to achieve the desired morphological, structural and functional properties of the targeted structures. For this reason, a parametric study was initially performed to determine the optimal range of the discharge’s externally controllable parameters (precursor and argon gas fluxes and microwave power) for the synthesis of graphene. The ethanol partial fluxes have been varied in the range 0.5–3.5 sccm. The evolving shape of the synthesized nanostructures, with changes of partial ethanol flow and microwave power delivered to the

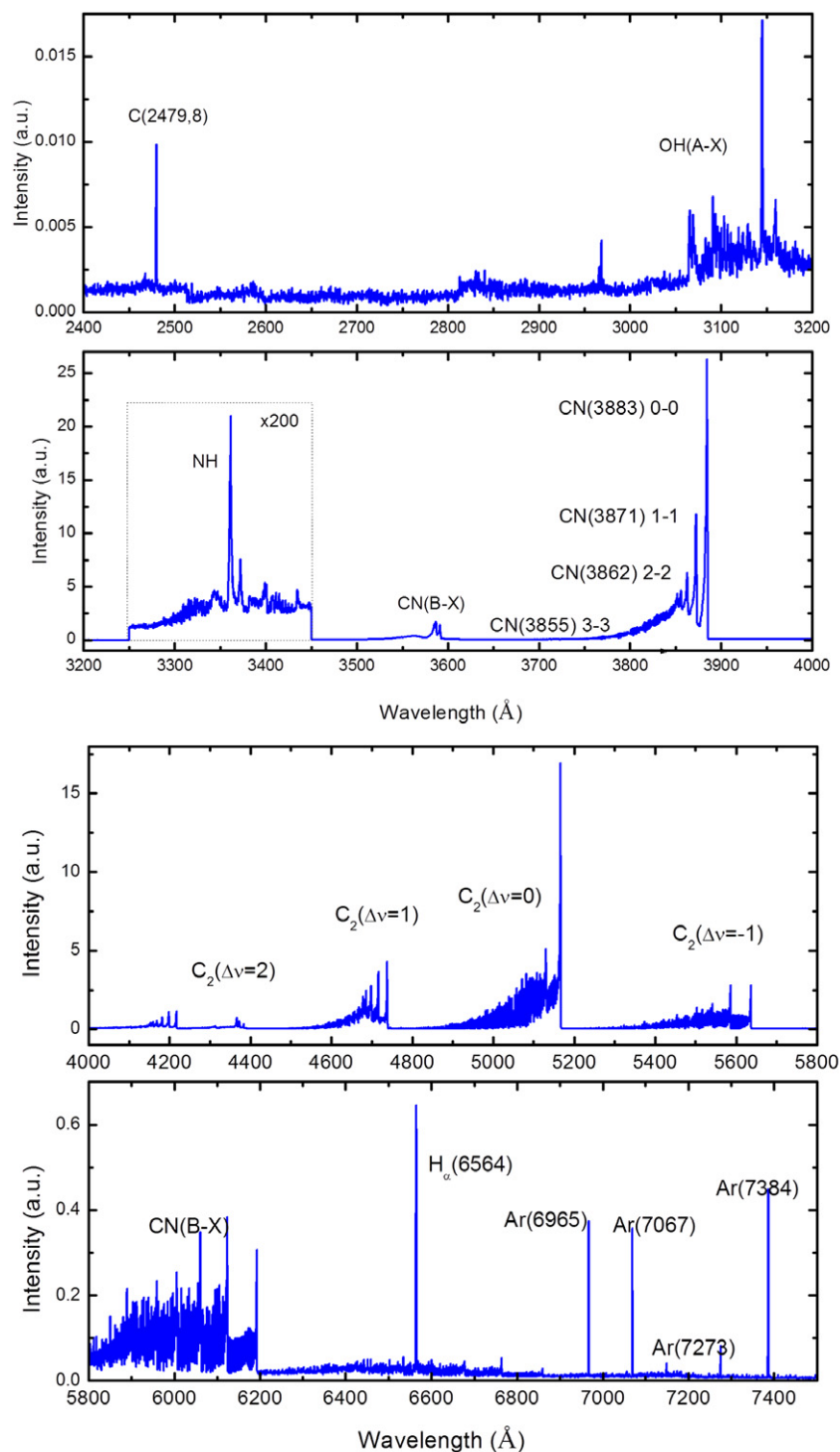


**Figure 3.** Plasma emission spectra ( $P = 500$  W,  $\Phi_{Ar} = 250$  sccm,  $\Phi_{Et} = 0.6$  sccm).

launcher, is shown in figure 4. The total gas flow was kept constant at 250 sccm. The collection time of the samples,  $\Delta t$ , was in the range 15–30 min. The SEM observation allowed us to make the following conclusions: for small partial ethanol fluxes (e.g., 0.6 sccm) and a microwave power of 500 W, carbon nanosheets resembling graphene are synthesized. For higher partial ethanol fluxes (3.6 sccm) amorphous nanostructures are produced. As expected, the density of carbon species decreases as the partial flux decreases, and, as a result, the conditions in

the assembly zone favored creation of planar nanostructures. That is, the existence of a smaller amount of nuclei surpassing the critical size for nucleation and growth, and conditions in which no supersaturation of species is possible given the limited flux, promote the growth of existing nuclei rather than the creation of new seeds.

Decreasing the microwave power from 500 to 400 W at a fixed ethanol flow (0.6 sccm) results in the production of nanoparticles with sizes ranging from 15 to 30 nm.

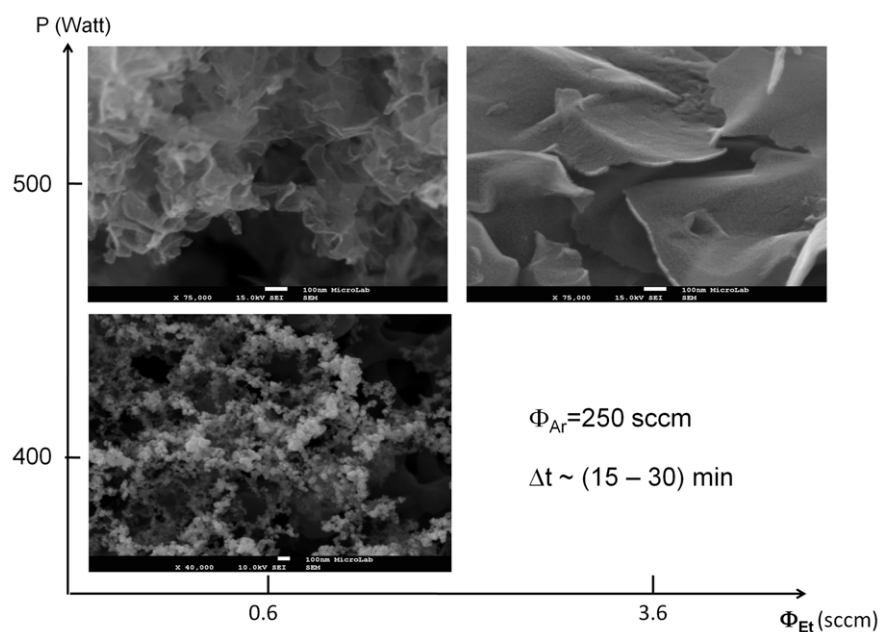


**Figure 4.** Nanostructure design versus ethanol partial flux and microwave power applied.

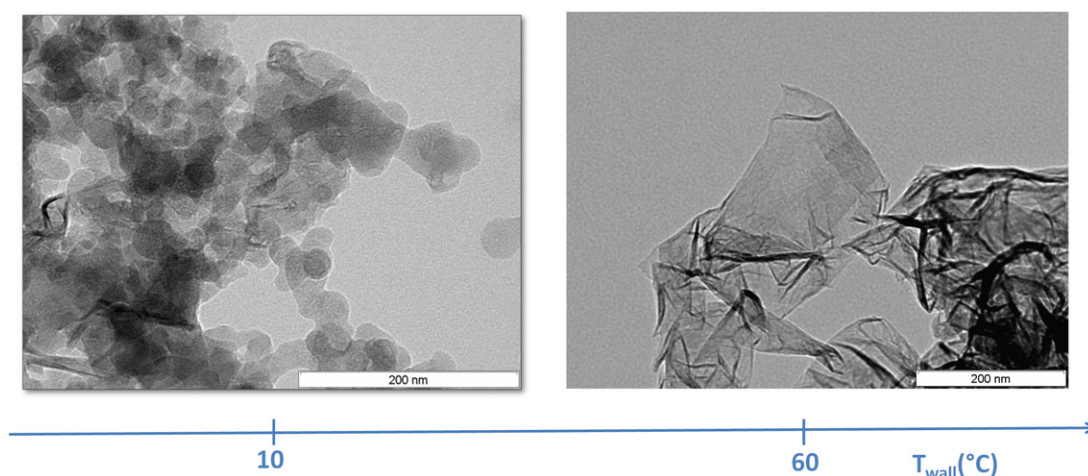


**Figure 5.** Nanostructure shape variation with wall temperature ( $P = 500 \text{ W}$ ,  $\Phi_{Ar} = 250 \text{ sccm}$ ,  $\Phi_{Et} = 0.6 \text{ sccm}$ ).

When the power decreases the gas temperature also decreases; consequently, supersaturation conditions are more likely to be created and the synthesis of multiple, homogeneously sized spherical structures is favored. Amorphous structures have been synthesized at higher ethanol partial fluxes.

As shown in [21] the temperature profile in the assembly zone can strongly influence the final product structure. For example, too long a residence time in this zone may result in growth of the  $sp^2$  planes, but graphene sheets can also agglomerate due to van der Waals interactions and form graphite. The evolution in the morphology of the synthesized nanostructures when the wall temperature in the assembly zone varies in the range 10–60 °C is shown in figure 5. A mixture of nearly spherical particles, with diameters up to about 50 nm, and nanosheets is observed when the wall temperature is set at 10 °C. At the temperature of 60 °C extended sheets are the only nanometric structures present. This reduction of the Gibbs

free energy of a saturated environment (gas + solid phase) is proportional to the gas temperature. Lower gas temperatures as well as large amounts of precursors foster supersaturation conditions in the environment (gas + solid phase) and thus promote the synthesis of plenty of multiple nuclei, while higher temperatures (and lower precursor amounts) favour the appearance of less nuclei and, consequently, a deviation from supersaturation conditions, more prone to generate graphitic sheets. The temperature profile in the assembly zone strongly impacts the final product structure. For example, too long a residence time in this zone might result in too much growth, thus allowing graphene structures to agglomerate and form graphite. Aiming at planar nanostructures, all further experiments have been conducted with fixed values of the gas fluxes, viz.,  $\Phi_{Ar} = 250 \text{ sccm}$  and  $\Phi_{Et} = 0.6 \text{ sccm}$  and changing only the microwave power and the wall temperature in the assembly zone.

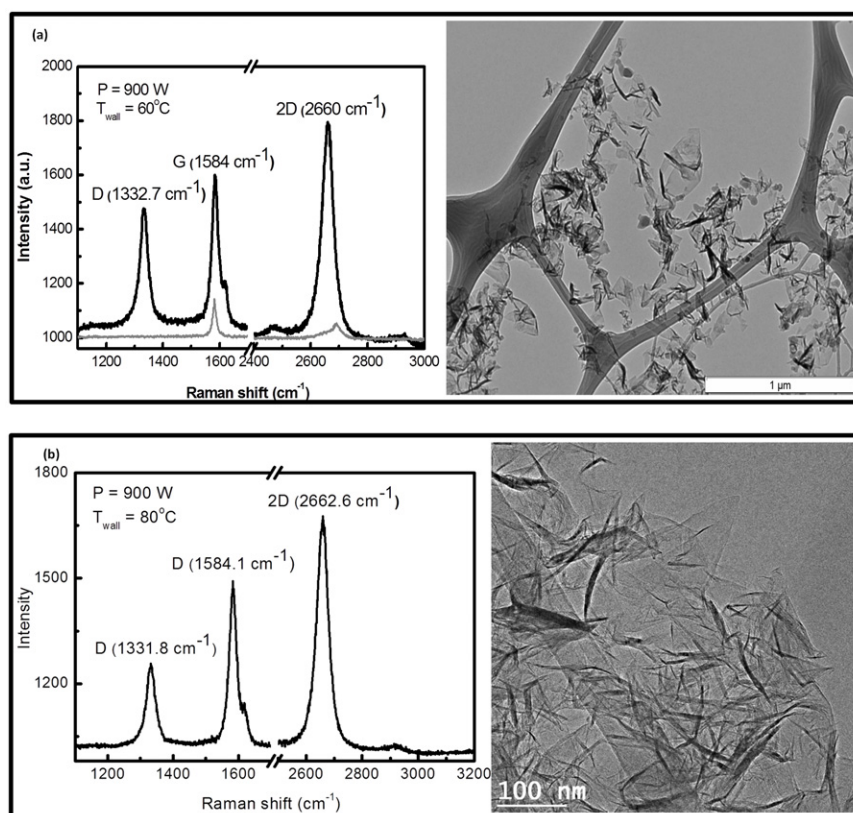


**Figure 6.** Raman spectra and corresponding low magnification TEM images of the sheets synthesized at microwave power  $P = 900$  W and different wall temperatures in the nucleation zone. (a)  $T_{\text{wall}} = 60^\circ\text{C}$ ; (b)  $T_{\text{wall}} = 80^\circ\text{C}$  ( $\Phi_{\text{Ar}} = 250$  sccm,  $\Phi_{\text{Et}} = 0.6$  sccm).

### 3.3. Raman and HRTEM analysis

The Raman spectra and low magnification TEM images of the synthesized carbon sheets at 900 W microwave power and two different wall temperatures 60 and  $80^\circ\text{C}$  are shown in figures 6(a) and (b). Graphene sheets collected on the filters (the filter with graphene is shown in figure 1 on the right upper corner) were freely suspended on the carbon grids for electron microscopy analysis. Note that the graphene sheets were found to be stable at atmospheric conditions. As seen in these images, there are sections in which the microstructural features are dominated by what appear to be single sheets and regions where folding and overlapping sheets, likely few-layer graphene, are observed. The darker areas are a result of crumpled regions. Further evidence for this was found from Raman spectroscopy.

In order to perform the Raman spectroscopy characterization, the synthesized nanostructures were freely suspended on a glass substrate and the Raman spectra from different regions on the substrate were obtained. Typical Raman spectra are shown in figures 6(a) and (b). As seen in figure 6(a), the sheets exhibit a sharp two-dimensional (2D) peak at about  $2660\text{ cm}^{-1}$  due to the second order process and a G-band peak due to the tangential zone centre mode at  $1584\text{ cm}^{-1}$  [29]. This type of Raman spectra has often been associated with graphene and provides evidence that the obtained nanosheets are indeed graphene. For comparison, Raman spectra of graphite powder are also shown with grey lines. As seen, there are significant changes in shape and intensity of the 2D peak of graphene

as compared to the graphite one. The 2D peak of graphite is much less intense, with a rather large full-width at half maximum (FWHM), while for graphene it is a single sharp peak red shifted in respect to that of graphite. The appearance of the D-peak at  $\sim 1333\text{ cm}^{-1}$  and the small shoulder of the G-peak at  $\sim 1620\text{ cm}^{-1}$  can be considered as a result of structural disorders, presence of  $\text{sp}^3$  carbons in the created sheets and/or edge effects [29].

The most prominent feature in the Raman spectrum of graphene is the 2D peak, whose position, shape and intensity are frequently used to distinguish between single-layer, bi-layer and multi-layer graphene. Taking into account the ratio between the 2D and G-peak integral intensities ( $>2$ ) and the FWHM of the 2D-band ( $\sim 45\text{ cm}^{-1}$ ) the obtained results can be interpreted as an indication of few-layer graphene synthesis. As shown in figures 7(a) and (b) the ratios of the disorder D-peak to the G-peak intensities and of the G-peak to the 2D-peak intensities decrease with increasing the wall temperature in the range  $60\text{--}100^\circ\text{C}$ .

The graphene nanosheets have been further characterized by high-resolution TEM (HRTEM), which was performed with a Titan ChemiStem (FEI) HRTEM operating at 200 kV. Figures 8(a) and (b) shows the HRTEM images of graphene sheets synthesized at 900 W microwave power and wall temperature of 60 and  $80^\circ\text{C}$ . The evident upward curling at the edges of the individual flakes may be due to internal stress in the few-layer graphene; these edges make it possible to evaluate the thicknesses of the sheets. As seen from the images, single- (1L) and few- (2L–7L) layer graphene sheets



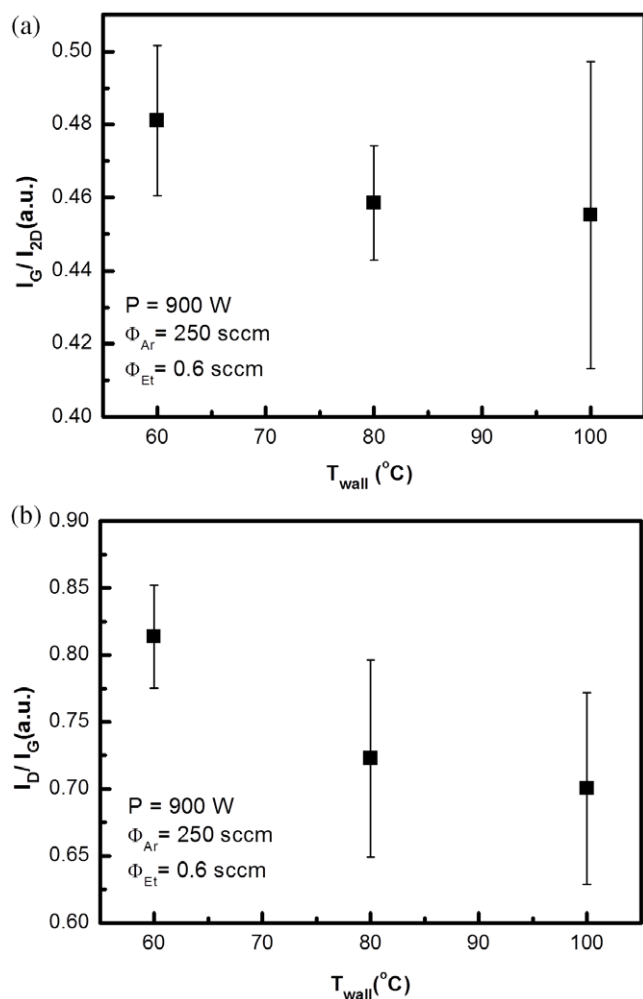


**Figure 7.** Ratio of the integrated intensities of G to 2D-peaks (a) and G to D-peaks (b) versus wall temperature in the assembly zone of the plasma reactor.

can be easily distinguished in the samples synthesized at 60 °C wall temperature. Moreover, highly ordered lattice fringes can be observed, indicating that the graphene sheets are well-crystallized (figure 8(a)). The graphene images shown in figure 8(b) demonstrate single-layer graphene sheets as well as bi-layer and three-layer graphene. The latter were synthesized at 900 W microwave power and wall temperature of 80 °C. The reduction in the number of mono-layers for higher wall temperatures in the assembly zone of the plasma reactor was noticed.

### 3.4. XPS analysis

The survey XPS spectrum (figure 9) is representative of all the samples and shows mainly the presence of carbon and of a relatively small amount of oxygen. The C 1s XPS detailed region and the corresponding energy loss features are shown in figure 10 for different wall temperatures in the assembly zone. As clearly seen in figure 10(a), C 1s is dominated by the peak centred at 284.4 eV, with  $\text{FWHM} = 1.0 \pm 0.1$  eV. Also,  $\text{sp}^3$  carbons ( $285.2 \pm 0.2$  eV) and carbon atoms bound to oxygen are detected: peaks centred at  $286.2 \pm 0.2$  eV,  $287.2 \pm 0.3$  and

$288.0 \pm 0.2$  eV are assigned to C–O, epoxide groups and C=O or O–C–O, respectively (table 1) [30]. The O 1s XPS region (not shown but described in table 1) is composed of two main peaks centred at 532.1 and  $533.7 \pm 0.1$  eV which correspond to oxygen in C=O and O–C=O or –OC–O–CO– groups, respectively [30, 31].

As it can be seen from the elemental analysis data presented in table 1, the percentage of  $\text{sp}^2$  hybridization increases when the wall temperature in the nucleation zone increases. Moreover, the obtained graphene samples are less oxidized, i.e., a loss of oxygen functionalities is observed. Thus, the control of the thermodynamic conditions in the assembly zone of the reactor results in improved structural quality of the fabricated nanostructures.

The C 1s energy loss region (figure 10(b)) includes some features assigned to energy losses: peaks around 6 eV from the main peak, centred at 284.4 eV and a wide band with a maximum at  $\sim 25$ –27 eV from the main peak. This broad band results from  $\sigma + \pi$  excitations and is centred around 27.0 eV for samples prepared with wall temperatures of 100 and 80 °C and at a slightly lower energy of  $\sim 25$  eV for  $T_{\text{wall}} = 60$  °C. These loss features are typical of graphite-like structures, like carbon nanotubes [32–34]. Peaks at  $\sim 6$  eV are attributed to  $\pi - \pi^*$  collective excitations. This low energy transition is common in strongly delocalized  $\pi$  electrons. While in graphene prepared with  $T_{\text{wall}} = 100$  °C the most intense peak is at 5.8 eV and it is at  $\sim 4.7$  eV in the  $T_{\text{wall}} = 100$  samples prepared with lower  $T_{\text{wall}}$ , i.e., a shift of  $\pi$  electron delocalization towards higher energies is observed.

All these results show that the sample prepared with  $T_{\text{wall}} = 100$  °C presents the largest value for the  $\text{sp}^2/\text{sp}^3$  ratio (which is larger than 1 for all the samples) and the lowest oxidation among the three samples ( $\text{C/O} = 18.4$ ) analysed. Thus, the results reveal loss of oxygen functionalities when the wall temperature in the assembly zone increases.

## 4. Conclusions

Self-standing graphene sheets were successfully synthesized using microwave plasmas driven by surface waves at 2.45 GHz stimulating frequency and at atmospheric pressure conditions. This method is based on injecting ethanol molecules through a microwave argon plasma environment, where decomposition of ethanol molecules takes place and carbon atoms are created. The evolution of the ethanol decomposition was studied *in situ* by plasma emission spectroscopy. Gas-phase carbon atoms diffuse into colder zones, both in radial and axial directions, and as a result gas-phase carbon is transformed into solid carbon nuclei. The main part of the solid carbon is gradually withdrawn from the hot region of the plasma in the outlet plasma stream where nanostructures assemble and grow. Since the temperature of the outlet plasma stream is a key parameter for the nucleation and growth processes, externally forced heating in the assembly zone of the plasma reactor has been applied to control the structural quality of the synthesized graphene sheets.

The fabricated graphene sheets are stable and highly ordered. The variation of the wall temperature in the assembly

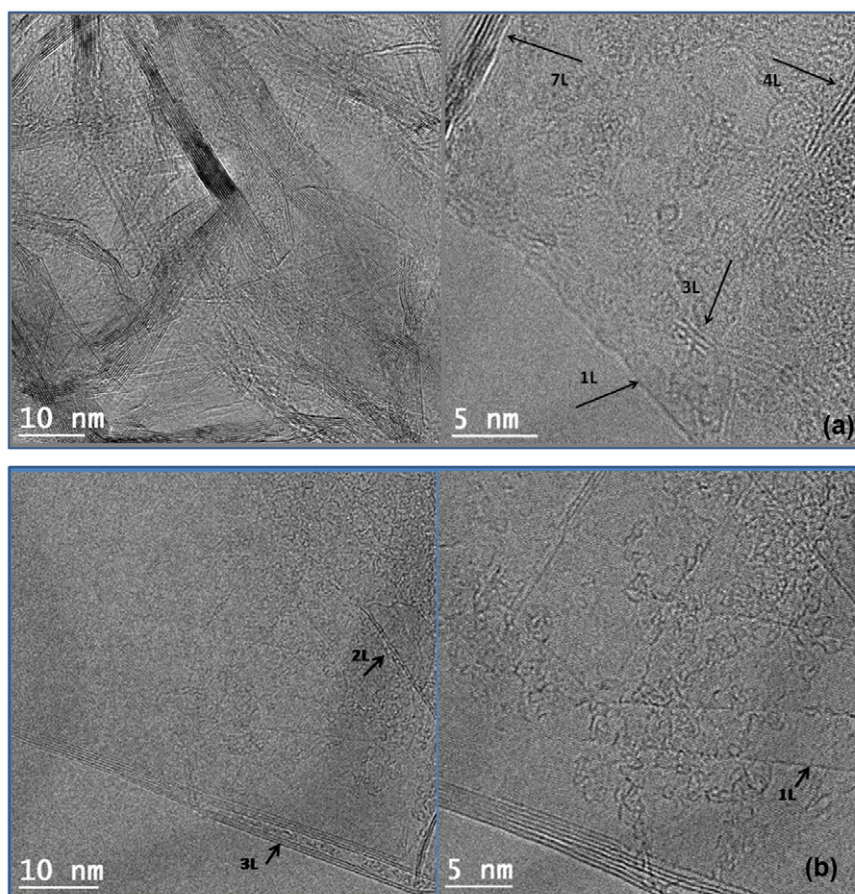


**Figure 8.** (a) HRTEM images of freely suspended graphene obtained at microwave power  $P = 900$  W and different wall temperatures: (a)  $T_{\text{wall}} = 60$  °C; (b)  $T_{\text{wall}} = 80$  °C; (b) ( $\Phi_{\text{Ar}} = 250$  sccm,  $\Phi_{\text{Et}} = 0.6$  sccm). Zones with few-layer graphene are marked with arrows.

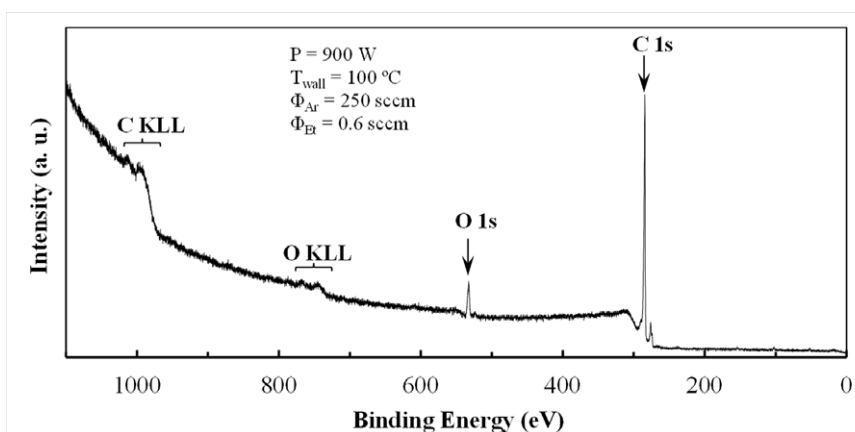
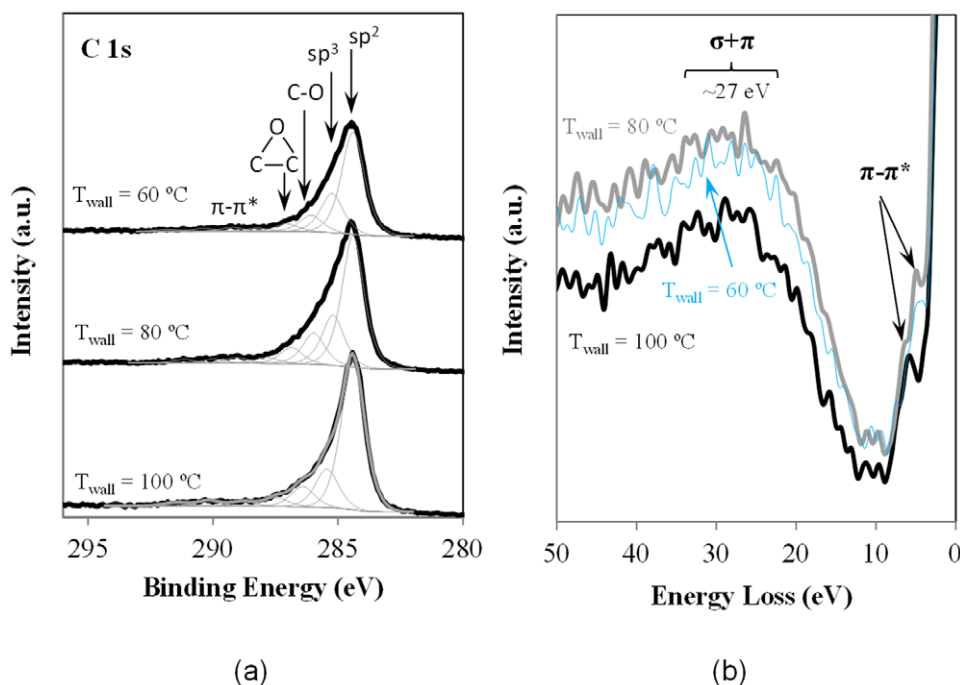


**Figure 9.** Survey XPS spectrum of the sample obtained at  $P = 900$  W and wall temperature 100 °C.

zone of the plasma reactor from 60 to 100 °C results in a change of their structural qualities. As Raman spectroscopy analysis demonstrates, the ratio of the disorder D-peak to the G-peak intensities decreases when the gas temperature of the outlet stream increases. At the same time, the percentage of  $sp^2$  hybridization increases and less oxygen functionalities are present in the graphene samples as shown by XPS elemental analysis. Therefore, the graphene structural quality can be controlled by changing the microwave power or/and by mastering the thermodynamic conditions via externally forced

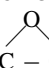
heating of the assembly zone of plasma reactor. The obtained sheets exhibit a structural quality comparable to that of existing graphene materials, but they are synthesized here without the need of metal or crystal substrates. A few milligrams graphene can be obtained for minutes at a single step at atmospheric pressure conditions. The results obtained here demonstrate that this method paves a reliable, versatile way towards scalable production of graphene structures for numerous applications.

By optimizing the microwave plasma reactor performance by concerning the gas flow regime (i.e., laminar or vortex flow),



**Figure 10.** C 1s XPS spectra (a) and energy loss features (b) obtained at different wall temperatures and supplied microwave power of 900 W.

**Table 1.** Peak positions and corresponding assignment, and relative amounts of carbon and oxygen atoms of graphene samples synthesized at different values of  $T_{\text{wall}}$ .

$T_{\text{wall}}$	BE ( $\pm 0.2$ eV)			Assignment	At. Conc. (%)		
	60 °C	80 °C	100 °C		60 °C	80 °C	100 °C
C 1s	284.4	284.4	284.4	$sp^2$ carbon	57.2	52.9	65.5
	285.2	285.2	285.4	$sp^3$ carbon	21.9	20.2	16.7
	286.1	286.0	286.4	C-O	9.4	12.5	8.8
	287.0	286.9	287.5	 C-C	4.3	6.4	3.8
O 1s	288.2	287.9		O-C-O or C=O	1.8	2.4	
	532.1	532.1	532.1	aliphatic C=O	2.3	1.2	3.3
	533.6	533.7	533.7	O-C=O or -OC-O-CO-	3.0	4.3	1.9
				Atomic ratios			
			$sp^2/sp^3$ carbons	2.6	2.6	3.9	
			C/O	17.8	17.0	18.4	

background gas mixture used, type of precursors, discharge geometry (by using, e.g. large scale discharge configurations) [35,36] and the thermodynamic conditions in the assembly zone, well controlled synthesis of carbon atom lattices can be achieved. Investigations along these directions are on-going in order to develop this graphene fabrication technique further.

### Acknowledgment

Work was partially supported by Fundação para a Ciência e a Tecnologia (Project Pest-OE/SADG/LA0010/2013).

### References

- [1] Meyer J C, Geim A K, Katsnelson M I, Novoselov K S, Booth T J and Roth S 2007 The structure of suspended graphene sheets *Nature* **446** 60
- [2] Wu Y H, Yu T and Shen Z X 2010 Two-dimensional carbon nanostructures: fundamental properties, synthesis, characterization, and potential applications *J. Appl. Phys.* **108** 071301
- [3] Gunho J, Minhyeok Ch, Sangchul L, Woojin P, Kahng Y H and Takhee L 2012 The application of graphene as electrodes in electrical and optical devices *Nanotechnology* **23** 112001
- [4] Phillips J, Luhrs C C and Richard M 2009 Review: engineering particles using the aerosol-through-plasma method *IEEE Trans. Plasma Sci.* **37** 726
- [5] Yurum Y, Taralp A and Veziroglu N 2009 Storage of hydrogen in nanostructured carbon materials *Int. J. Hydrogen Energy* **34** 3784
- [6] Choi H, Jung S, Seo J, Chang D W, Dai L and Baek J 2012 Graphene for energy conversion and storage in fuel cells and supercapacitors *Nano Energy* **1** 534
- [7] Mao S, Pu H and Chen J 2012 Graphene oxide and its reduction: modeling and experimental progress *RSC Adv.* **2** 2643

- [8] Reina A, Jia X, Ho J, Nezich D, Son H, Bulovic V, Dresselhaus M S and Kong J 2009 Few-layer graphene films on arbitrary substrates by chemical vapor deposition *Nano Lett.* **9** 30
- [9] Gannett W, Regan, Watanabe K, Taniguchi T, Crommie M F and Zettl A 2011 Boron nitride substrates for high mobility chemical vapor deposited graphene *Appl. Phys. Lett.* **98** 242105
- [10] Garaj S, Hubbard W and Golovchenko J A 2010 Graphene synthesis by ion implantation *Appl. Phys. Lett.* **97** 183103
- [11] Yamada T, Kim J, Ishihara M and Hasegawa M 2013 Low-temperature graphene synthesis using microwave plasma CVD *J. Phys. D: Appl. Phys.* **46** 063001
- [12] Ostrikov K, Cvelbar U and Murphy A B 2011 Plasma nanoscience: setting directions, tackling grand challenges *J. Phys. D: Appl. Phys.* **44** 174001
- [13] Levchenko I, Keidar M, Xu S, Kersten H and Ostrikov K 2013 Low-temperature plasmas in carbon nanostructure synthesis *J. Vac. Sci. Technol. B* **31** 050801
- [14] Nandamuri G, Roumimov S and Solanki R 2010 Remote plasma assisted growth of graphene films *Appl. Phys. Lett.* **96** 154101
- [15] Chou C H and Phillips J 1992 Plasma production of metallic nanoparticles *J. Mater. Res.* **7** 2107
- [16] Phillips J, Shim S, Fonseca I M and Carabineiro S 2002 Plasma generation of supported metal catalysts *Appl. Catal.* **237** 41
- [17] Chen C K, Perry V W and Phillips J 2002 Plasma torch production of macroscopic carbon nanotube structures *Carbon* **41** 2555
- [18] Lambert T N, Luhrs C C, Chavez C A, Wakeland S, Brumbach M T and Alam T M 2010 Graphite oxide as a precursor for the synthesis of disordered graphenes using the aerosol-through-plasma method *Carbon* **48** 4081
- [19] Luhrs, Wakeland S and Carpenter B 2012 Graphene, graphitic and amorphous carbon nanostructures generation by atmospheric microwave plasma method *Plasma for Environmental Issues* ed E Tatarova et al (Sofia: Artgraf) pp 69–80 (ISBN 978-954-9401-63-9)
- [20] Dato A, Radmilovic V, Lee Z, Phillips J and Frenklach M 2008 Substrate-free gas-phase synthesis of graphene sheets *Nano Lett.* **8** 2012
- [21] Tatarova E, Henriques J P, Luhrs C C, Dias A, Phillips J, Abrashev M V and Ferreira C M 2013 Microwave plasma based single step method for free standing graphene synthesis at atmospheric conditions *Appl. Phys. Lett.* **103** 134101
- [22] Mowry M, Palaniuk D, Luhrs C C and Osswald S 2013 *In situ* Raman spectroscopy and thermal analysis of the formation of nitrogen-doped graphene from urea and graphite oxide *RSC Adv.* **3** 21763–75
- [23] Moisan M and Zakrzewski Z 1991 Plasma sources based on the propagation of electromagnetic surface waves *J. Phys. D: Appl. Phys.* **24** 1025
- [24] Tatarova E, Dias F M, Henriques J P, Felizardo E, Ferreira C M and Gordiets B 2008 Microwave plasma torches driven by surface waves *Plasma Sources Sci. Technol.* **702** 4004
- [25] Henriques J P, Tatarova E, Dias F M and Ferreira C M 2011 Microwave N<sub>2</sub>-Ar plasma torch: experiment and comparison with theory *J. Appl. Phys.* **109** 023302
- [26] Tatarova E, Bundaleska N, Dias F M, Tsyganov D, Saavedra R and Ferreira C M 2013 Hydrogen production from alcohol reforming in a microwave ‘tornado’-type plasma *Plasma Sources Sci. Technol.* **22** 065001
- [27] Timmermans E A H, Jonkers J, Rodero A, Quintero M C, Sola A, Gamero A 1999 The behavior of molecules in microwave-induced plasmas studied by optical emission spectroscopy: II. Plasmas at reduced pressure *Spectrochim. Acta* **54** 1085
- [28] Tatarova E, Henriques J P, Felizardo E, Lino da Silva M, Ferreira C M and Gordiets B 2012 Microwave plasma source operating with atmospheric pressure air–water mixtures *J. Appl. Phys.* **112** 093301
- [29] Ferrari A C et al 2006 Raman spectrum of graphene and graphene layers *Phys. Rev. Lett.* **97** 187401
- [30] Beamson G and Briggs D 1992 *High Resolution XPS of Organic Polymers* The Scienta ESCA300 Database (New York: John Wiley)
- [31] Botelho do Rego A M, Ferraria A M, Rei Vilar M and Boufi S 2013 X-ray photoelectron spectroscopy: a tool for studying biopolymers *Handbook of Biopolymer-based Materials: From Blends and Composites to Gels and Complex Networks* vol 2, ed Thomas et al (Weinheim: Wiley-VCH Verlag)
- [32] Chen P, Wu X, Sun X, Lin J, Ji W and Tan K L 1999 Electronic structure and optical limiting behavior of carbon nanotubes *Phys. Rev. Lett.* **82** 2548
- [33] Fink J, Muller-Heinzerling Th, Pfluger J, Scheerer B, Dischler B, Koidl P, Bubenzer A and Sah R I 1984 Investigation of hydrocarbon-plasma-generated carbon films by electron-energy-loss spectroscopy *Phys. Rev. B* **30** 4713
- [34] Ajayan P M, Iijima S and Ichihashi T 1993 Electron-energy-loss spectroscopy of carbon nanometer-size tubes *Phys. Rev. B* **47** 6859
- [35] Tatarova E, Henriques J P, Dias F M and Ferreira C M 2006 Large-scale Ar and N<sub>2</sub>-Ar microwave plasma sources *J. Phys. D: Appl. Phys.* **39** 2747
- [36] Henriques J P, Tatarova E, Dias F M and Ferreira C M 2008 Spatial structure of a slot-antenna excited microwave N<sub>2</sub>-Ar plasma source *J. Appl. Phys.* **103** 103304